massachusetts institute of technology — artificial intelligence laboratory

Nonparametric Belief Propagation and Facial Appearance Estimation

Erik B. Sudderth, Alexander T. Ihler,
William T. Freeman and Alan S. Willsky

AI Memo 2002-020 December 2002

Abstract

In many applications of graphical models arising in computer vision, the hidden variables of interest are most naturally specified by continuous, non-Gaussian distributions. There exist inference algorithms for discrete approximations to these continuous distributions, but for the high-dimensional variables typically of interest, discrete inference becomes infeasible. Stochastic methods such as particle filters provide an appealing alternative. However, existing techniques fail to exploit the rich structure of the graphical models describing many vision problems.

Drawing on ideas from regularized particle filters and belief propagation (BP), this paper develops a nonparametric belief propagation (NBP) algorithm applicable to general graphs. Each NBP iteration uses an efficient sampling procedure to update kernel-based approximations to the true, continuous likelihoods. The algorithm can accomodate an extremely broad class of potential functions, including nonparametric representations. Thus, NBP extends particle filtering methods to the more general vision problems that graphical models can describe. We apply the NBP algorithm to infer component interrelationships in a parts-based face model, allowing location and reconstruction of occluded features.

This report describes research done within the Laboratory for Information and Decision Systems and the Artificial Intelligence Laboratory at the Massachusetts Institute of Technology. This research was supported in part by ONR under Grant N00014-00-1-0089, by AFOSR under Grant F49620-00-1-0362, and by an ODDR&E MURI funded through ARO Grant DAAD19-00-1-0466. E. S. was partially funded by an NDSEG fellowship.

1. Introduction

Graphical models provide a powerful, general framework for developing statistical models of computer vision problems [7, 9, 10]. However, graphical formulations are only useful when combined with efficient algorithms for inference and learning. Computer vision problems are particularly challenging because they often involve high–dimensional, continuous variables and complex, multimodal distributions. For example, the articulated models used in many tracking applications have dozens of degrees of freedom to be estimated at each time step [18]. Realistic graphical models for these problems must represent outliers, bimodalities, and other non–Gaussian statistical features. The corresponding optimal inference procedures for these models typically involve integral equations for which no closed form solution exists. Thus, it is necessary to develop families of approximate representations, and corresponding methods for updating those approximations.

The simplest method for approximating intractable continuous–valued graphical models is discretization. Although exact inference in general discrete graphs is NP hard [2], approximate inference algorithms such as loopy belief propagation (BP) [17, 22, 24, 25] have been shown to produce excellent empirical results in many cases. Certain vision problems, including stereo vision [21] and phase unwrapping [8], are well suited to discrete formulations. For problems involving high–dimensional variables, however, exhaustive discretization of the state space is intractable. In some cases, domain–specific heuristics may be used to dynamically exclude those configurations which appear unlikely based upon the local evidence [3, 7]. In more challenging vision applications, however, the local evidence at some nodes may be inaccurate or misleading, and these approaches will heavily distort the computed estimates.

For temporal inference problems, particle filters [6, 10] have proven to be an effective, and influential, alternative to discretization. They provide the basis for several of the most effective visual tracking algorithms [15, 18]. Particle filters approximate conditional densities nonparametrically as a collection of representative elements. Although it is possible to update these approximations deterministically using local linearizations [1], most implementations use Monte Carlo methods to stochastically update a set of weighted point samples. The stability and robustness of particle filters can often be improved by regularization methods [6, Chapter 12] in which smoothing kernels [16, 19] explicitly represent the uncertainty associated with each point sample.

Although particle filters have proven to be extremely effective for visual tracking problems, they are specialized to temporal problems whose corresponding graphs are simple Markov chains (see Figure 1). Many vision problems, however, are characterized by non–causal (e.g., spatial or model–induced) structure which is better represented by a more complex graph. Because particle filters cannot be applied to arbitrary graphs, graphical models containing high–dimensional variables may pose severe problems for existing inference techniques. Even for tracking problems, there is often structure within each time instant (for example, associated with an articulated model) which is ignored by standard particle filters.

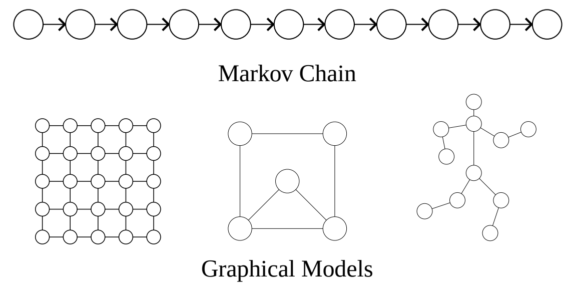

Figure 1: Particle filters assume variables are related by a simple Markov chain. The NBP algorithm extends particle filtering techniques to arbitrarily structured graphical models.

Some authors have used junction tree representations [12] to develop structured approximate inference techniques for general graphs. These algorithms begin by clustering nodes into cliques chosen to break the original graph's cycles. A wide variety of algorithms can then be specified by combining an approximate clique variable representation with local methods for updating these approximations [4, 11]. For example, Koller et al. [11] propose a framework in which the current clique potential estimate is used to guide message computations, allowing approximations to be gradually refined over successive iterations. However, the sample algorithm they provide is limited to networks containing mixtures of discrete and Gaussian variables. In addition, for many graphs (e.g. nearest–neighbor grids) the size of the junction tree's largest cliques grows exponentially with problem size, requiring the estimation of extremely high–dimensional distributions.

The *nonparametric belief propagation* (NBP) algorithm we develop in this paper differs from previous nonparametric approaches in two key ways. First, for graphs with cycles we do *not* form a junction tree, but instead iterate our local message updates until convergence as in loopy BP. This has the advantage of greatly reducing the dimensionality of the spaces over which we must infer distributions. Second, we provide a message update algorithm specifically adapted to graphs containing continuous, non–Gaussian potentials. The primary difficulty in extending particle filters to general graphs is in determining efficient methods for combining the information provided by several neighboring nodes. Representationally, we address this problem by associating a regularizing kernel with each particle, a step which is necessary to make message products well defined. Computationally, we show that message products may be computed using an efficient *local* Gibbs sampling procedure. The NBP algorithm may be applied to arbitrarily structured graphs containing a broad range of potential functions, effectively extending particle filtering methods to a much broader range of vision problems.

Following our presentation of the NBP algorithm, we validate its performance on a small Gaussian network. We then show how NBP may be combined with parts–based local appearance models [5, 14, 23] to locate and reconstruct occluded facial features.

2. Undirected Graphical Models

An undirected graph $\mathcal{G}$ is defined by a set of nodes $\mathcal{V}$, and a corresponding set of edges $\mathcal{E}$. The *neighborhood* of a node $s \in \mathcal{V}$ is defined as $\Gamma(s) \triangleq \{t|(s,t) \in \mathcal{E}\}$, the set of all nodes which are directly connected to s. Graphical models associate each node $s \in \mathcal{V}$ with an unobserved, or hidden, random variable x_s, as well as a noisy local observation y_s. Let $x = \{x_s\}_{s\in\mathcal{V}}$ and $y = \{y_s\}_{s\in\mathcal{V}}$ denote the sets of all hidden and observed variables, respectively. To simplify the presentation, we consider models with pairwise potential functions, for which $p(x, y)$ factorizes as

$$p(x,y) = \frac{1}{Z} \prod_{(s,t)\in\mathcal{E}} \psi_{s,t}(x_s, x_t) \prod_{s\in\mathcal{V}} \psi_s(x_s, y_s) \qquad (1)$$

However, the nonparametric updates we present may be directly extended to models with higher–order potential functions.

In this paper, we focus on the calculation of the conditional marginal distributions $p(x_s \mid y)$ for all nodes $s \in \mathcal{V}$. These densities provide not only estimates of x_s, but also corresponding measures of uncertainty.

2.1. Belief Propagation

For graphs which are acyclic or tree–structured, the desired conditional distributions $p(x_s \mid y)$ can be directly calculated by a local message–passing algorithm known as *belief propagation* (BP) [17, 25]. At iteration n of the BP algorithm, each node $t \in \mathcal{V}$ calculates a message $m^n_{ts}(x_s)$ to be sent to each neighboring node $s \in \Gamma(t)$:

$$m^n_{ts}(x_s) = \alpha \int_{x_t} \psi_{s,t}(x_s, x_t)\, \psi_t(x_t, y_t) \times \prod_{u\in\Gamma(t)\setminus s} m^{n-1}_{ut}(x_t)\, dx_t \qquad (2)$$

Here, α denotes an arbitrary proportionality constant. At any iteration, each node can produce an approximation $\hat{p}^n(x_s \mid y)$ to the marginal distributions $p(x_s \mid y)$ by combining the incoming messages with the local observation potential:

$$\hat{p}^n(x_s \mid y) = \alpha \psi_s(x_s, y_s) \prod_{t\in\Gamma(s)} m^n_{ts}(x_s) \qquad (3)$$

For tree–structured graphs, the approximate marginals, or beliefs, $\hat{p}^n(x_s \mid y)$ will converge to the true marginals $p(x_s \mid y)$ once the messages from each node have propagated to every other node in the graph.

Because each iteration of the BP algorithm involves only local message updates, it can be applied even to graphs with cycles. For such graphs, the statistical dependencies between BP messages are not properly accounted for, and the sequence of beliefs $\hat{p}^n(x_s \mid y)$ will *not* converge to the true marginal distributions. In many applications, however, the resulting loopy BP algorithm exhibits excellent empirical performance [7, 8]. Recently, several theoretical studies have provided insight into the approximations made by loopy BP, partially justifying its application to graphs with cycles [22, 24, 25].

2.2. Nonparametric Representations

Exact evaluation of the BP update equation (2) involves an integration which, as discussed in the Introduction, is not analytically tractable for most continuous hidden variables. An interesting alternative is to represent the resulting message $m_{ts}(x_s)$ nonparametrically as a kernel–based density estimate [16, 19]. Let $\mathcal{N}(x; \mu, \Lambda)$ denote the value of a Gaussian density of mean μ and covariance Λ at the point x. We may then approximate $m_{ts}(x_s)$ by a mixture of M Gaussian kernels as

$$m_{ts}(x_s) = \sum_{i=1}^{M} w_s^{(i)} \mathcal{N}\left(x_s; \mu_s^{(i)}, \Lambda_s\right) \qquad (4)$$

where $w_s^{(i)}$ is the weight associated with the i^{th} kernel mean $\mu_s^{(i)}$, and Λ_s is a bandwidth or smoothing parameter. Other choices of kernel functions are possible [19], but in this paper we restrict our attention to mixtures of diagonal–covariance Gaussians.

In the following section, we describe stochastic methods for determining the kernel centers $\mu_s^{(i)}$ and associated weights $w_s^{(i)}$. The resulting nonparametric representations are only meaningful when the messages $m_{ts}(x_s)$ are finitely integrable.[1] To guarantee this, it is sufficient to assume that all potentials satisfy the following constraints:

$$\begin{aligned} \int_{x_s} \psi_{s,t}(x_s, x_t = \bar{x})\, dx_s &< \infty \\ \int_{x_s} \psi_s(x_s, y_s = \bar{y})\, dx_s &< \infty \end{aligned} \qquad (5)$$

[1] Probabilistically, BP messages are likelihood functions $m_{ts}(x_s) \propto p(y = \bar{y} \mid x_s)$, not densities, and are *not* necessarily integrable (e.g., when x_s and y are independent).

Under these assumptions, a simple induction argument will show that all messages are normalizable. Heuristically, equation (5) requires all potentials to be "informative," so that fixing the value of one variable constrains the likely locations of the other. In most application domains, this can be trivially achieved by assuming that all hidden variables take values in a large, but bounded, range.

3. Nonparametric Message Updates

Conceptually, the BP update equation (2) naturally decomposes into two stages. First, the message product $\psi_t(x_t, y_t) \prod_u m_{ut}^{n-1}(x_t)$ combines information from neighboring nodes with the local evidence y_t, producing a function summarizing all available knowledge about the hidden variable x_t. We will refer to this summary as a likelihood function, even though this interpretation is only strictly correct for an appropriately factorized tree–structured graph. Second, this likelihood function is combined with the compatibility potential $\psi_{s,t}(x_s, x_t)$, and then integrated to produce likelihoods for x_s. The nonparametric belief propagation (NBP) algorithm stochastically approximates these two stages, producing consistent nonparametric representations of the messages $m_{ts}(x_s)$. Approximate marginals $\hat{p}(x_s \mid y)$ may then be determined from these messages by applying the following section's stochastic product algorithm to equation (3).

3.1. Message Products

For the moment, assume that the local observation potentials $\psi_t(x_t, y_t)$ are represented by weighted Gaussian mixtures (such potentials arise naturally from learning–based approaches to model identification [7]). The product of d Gaussian densities is itself Gaussian, with mean and covariance given by

$$\prod_{j=1}^{d} \mathcal{N}(x; \mu_j, \Lambda_j) \propto \mathcal{N}(x; \bar{\mu}, \bar{\Lambda})$$
$$\bar{\Lambda}^{-1} = \sum_{j=1}^{d} \Lambda_j^{-1} \qquad \bar{\Lambda}^{-1}\bar{\mu} = \sum_{j=1}^{d} \Lambda_j^{-1}\mu_j \tag{6}$$

Thus, a BP update operation which multiplies d Gaussian mixtures, each containing M components, will produce another Gaussian mixture with M^d components. The weight $\bar{w}$ associated with product mixture component $\mathcal{N}(x; \bar{\mu}, \bar{\Lambda})$ is given by

$$\bar{w} \propto \frac{\prod_{j=1}^{d} w_j \mathcal{N}(x; \mu_j, \Lambda_j)}{\mathcal{N}(x; \bar{\mu}, \bar{\Lambda})} \tag{7}$$

where $\{w_j\}_{j=1}^{d}$ are the weights associated with the input Gaussians. Note that equation (7) produces the same value for any choice of x. Also, in various special cases, such as when all input Gaussians have the same variance $\Lambda_j = \Lambda$, computationally convenient simplifications are possible.

Since integration of Gaussian mixtures is straightforward, in principle the BP message updates could be performed exactly by repeated use of equations (6,7). In practice, however, the exponential growth of the number of mixture components forces approximations to be made. Given d input mixtures of M Gaussian, the NBP algorithm approximates their M^d–component product mixture by drawing M independent samples.

Direct sampling from this product, achieved by explicitly calculating each of the product component weights (7), would require $\mathcal{O}(M^d)$ operations. The complexity associated with this sampling is combinatorial: each product component is defined by d labels $\{l_j\}_{j=1}^{d}$, where l_j identifies a kernel in the j^{th} input mixture. Although the joint distribution of the d labels is complex, the conditional distribution of any individual label l_j is simple. In particular, assuming fixed values for $\{l_k\}_{k \neq j}$, equation (7) can be used to sample from the conditional distribution of l_j in $\mathcal{O}(M)$ operations.

Since the mixture label conditional distributions are tractable, we may use a Gibbs sampler [9] to draw asymptotically unbiased samples from the product distribution. Details are provided in Algorithm 1, and illustrated in Figure 2. At each iteration, the labels $\{l_k\}_{k \neq j}$ for $d-1$ of the input mixtures are fixed, and a new value for the j^{th} label is chosen according to equation (7). At the following iteration, the newly chosen l_j is fixed, and another label is updated. This procedure continues for a fixed number of iterations κ; more iterations lead to more accurate samples, but require greater computational cost. Following the final iteration, the mean and covariance of the selected product mixture component is found using equation (6), and a sample point is drawn. To draw M (approximate) samples from the product distribution, the Gibbs sampler requires a total of $\mathcal{O}(d\kappa M^2)$ operations.

Although formal verification of the Gibbs sampler's convergence is difficult, in our experiments we have observed good performance using far fewer computations than required by direct sampling. Note that the NBP algorithm uses the Gibbs sampling technique differently from classic simulated annealing procedures [9]. In simulated annealing, the Gibbs sampler updates a single Markov chain whose state dimension is proportional to the graph dimension. In contrast, NBP uses many *local* Gibbs samplers, each involving only a few nodes. Thus, although NBP must run more independent Gibbs samplers, for large graphs the dimensionality of the corresponding Markov chains is dramatically smaller.

In some applications, the observation potentials $\psi_t(x_t, y_t)$ are most naturally specified by analytic functions. The previously proposed Gibbs sampler may

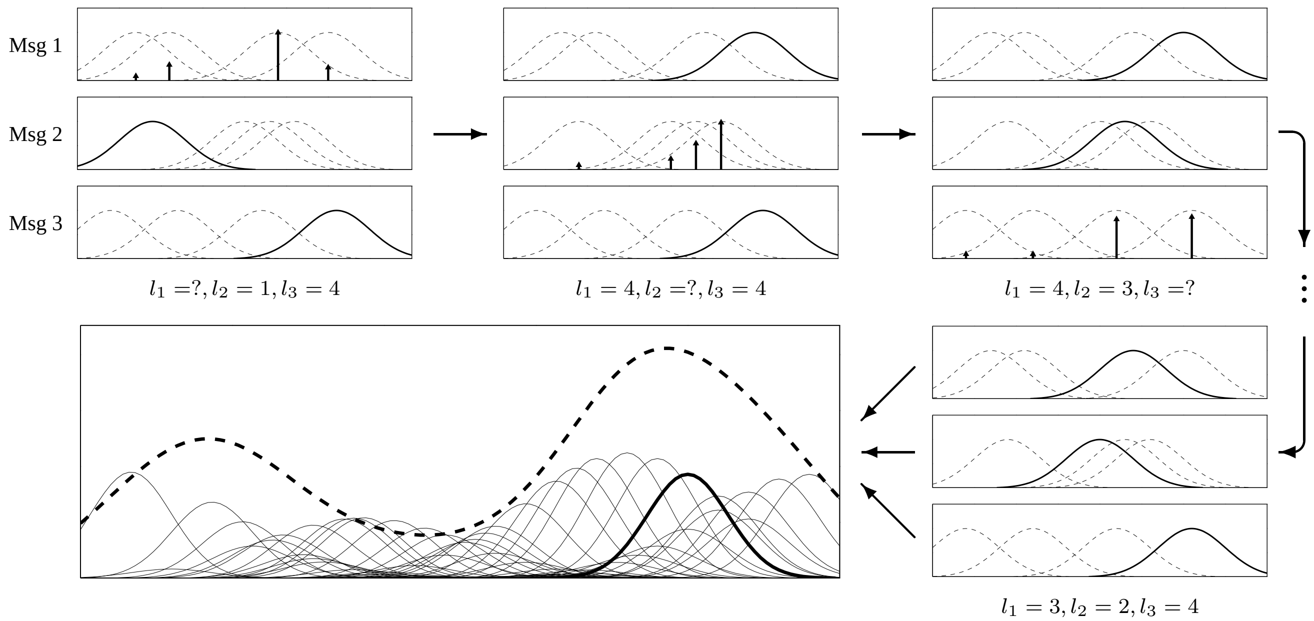

Figure 2: *Top row:* Gibbs sampler for a product of 3 Gaussian mixtures, with 4 kernels each. New indices are sampled according to weights (arrows) determined by the two fixed components (solid). The Gibbs sampler cycles through the different messages, drawing a new mixture label for one message conditioned on the currently labeled Gaussians in the other messages. *Bottom row:* After κ iterations through all the messages, the final labeled Gaussians for each message (right, solid) are multiplied together to identify one (left, solid) of the 4^3 components (left, thin) of the product density (left, dashed).

be easily adapted to this case using *importance sampling* [6], as shown in Algorithm 2. At each iteration, the weights used to sample a new kernel label are rescaled by $\psi_t\left(\bar{\mu}^{(i)}, y_t\right)$, the observation likelihood at each kernel's center. Then, the final sample is assigned an importance weight to account for variations of the analytic potential over the kernel's support. This procedure will be most effective when $\psi_t\left(x_t, y_t\right)$ varies slowly relative to the typical kernel bandwidth.

3.2. Message Propagation

In the second stage of the NBP algorithm, the information contained in the incoming message product is propagated by stochastically approximating the belief update integral (2). To perform this stochastic integration, the pairwise potential $\psi_{s,t}\left(x_s, x_t\right)$ must be decomposed to separate its *marginal* influence on x_t from the *conditional* relationship it defines between x_s and x_t.

The marginal influence function $\zeta(x_t)$ is determined by the relative weight assigned to *all* x_s values for each x_t:

$$\zeta(x_t) = \int_{x_s} \psi_{s,t}\left(x_s, x_t\right)\, dx_s \tag{8}$$

The NBP algorithm accounts for the marginal influence of $\psi_{s,t}\left(x_s, x_t\right)$ by incorporating $\zeta(x_t)$ into the Gibbs sampler. If $\psi_{s,t}\left(x_s, x_t\right)$ is a Gaussian mixture, extraction of $\zeta(x_t)$ is trivial. Alternately, if $\zeta(x_t)$ can be evaluated (or approximated) pointwise, analytic pairwise potentials may be dealt with using importance sampling. In the common case where pairwise potentials depend only on the difference between their arguments ($\psi_{s,t}\left(x, \bar{x}\right) = \psi_{s,t}\left(x - \bar{x}\right)$), $\zeta(x_t)$ is constant and can be neglected.

To complete the stochastic integration, each particle $x_t^{(i)}$ produced by the Gibbs sampler is propagated to node s by sampling $x_s^{(i)} \sim \psi_{s,t}(x_s, x_t^{(i)})$. Note that the assumptions of Section 2.2 ensure that $\psi_{s,t}(x_s, x_t^{(i)})$ is normalizable for any $x_t^{(i)}$. The method by which this sampling step is performed will depend on the specific functional form of $\psi_{s,t}\left(x_s, x_t\right)$, and may involve importance sampling or MCMC techniques. Finally, having produced a set of independent samples from the desired output message $m_{ts}\left(x_s\right)$, NBP must choose a kernel bandwidth to complete the nonparametric density estimate. There are many ways to make this choice; for the results in this paper, we used the computationally efficient "rule of thumb" heuristic [19].

The NBP message update procedure developed in this section is summarized in Algorithm 3. Note that various stages of this algorithm may be simplified in certain special cases. For example, if the pairwise potentials $\psi_{s,t}\left(x_s, x_t\right)$ are mixtures of only one or two Gaussians, it is possible to replace the sampling and kernel size selection of steps 3–4 by a simple deterministic kernel placement. However, Given d mixtures of M Gaussians, where $\{\mu_j^{(i)}, \Lambda_j^{(i)}, w_j^{(i)}\}_{i=1}^M$ denote the parameters of the j^{th} mixture:

1. For each $j \in [1:d]$, choose a starting label $l_j \in [1:M]$ by sampling $p(l_j = i) \propto w_j^{(i)}$.
2. For each $j \in [1:d]$,
   (a) Calculate the mean μ^* and variance Λ^* of the product $\prod_{k \neq j} \mathcal{N}\left(x; \mu_k^{(l_k)}, \Lambda_k^{(l_k)}\right)$ using equation (6).
   (b) For each $i \in [1:M]$, calculate the mean $\bar{\mu}^{(i)}$ and variance $\bar{\Lambda}^{(i)}$ of $\mathcal{N}(x; \mu^*, \Lambda^*) \cdot \mathcal{N}\left(x; \mu_j^{(i)}, \Lambda_j^{(i)}\right)$. Using any convenient x, compute the weight
   $$\bar{w}^{(i)} = w_j^{(i)} \frac{\mathcal{N}\left(x; \mu_j^{(i)}, \Lambda_j^{(i)}\right) \mathcal{N}(x; \mu^*, \Lambda^*)}{\mathcal{N}\left(x; \bar{\mu}^{(i)}, \bar{\Lambda}^{(i)}\right)}$$
   (c) Sample a new label l_j according to $p(l_j = i) \propto \bar{w}^{(i)}$.
3. Repeat step 2 for κ iterations.
4. Compute the mean $\bar{\mu}$ and variance $\bar{\Lambda}$ of the product $\prod_{j=1}^d \mathcal{N}\left(x; \mu_j^{(l_j)}, \Lambda_j^{(l_j)}\right)$. Draw a sample $\hat{x} \sim \mathcal{N}\left(x; \bar{\mu}, \bar{\Lambda}\right)$.

Algorithm 1: Gibbs sampler for products of Gaussian mixtures.

Given d mixtures of M Gaussians and an analytic function $f(x)$, follow Algorithm 1 with the following modifications:

2. After part (b), rescale each computed weight by the analytic value at the kernel center: $\bar{w}^{(i)} \leftarrow f(\bar{\mu}^{(i)})\bar{w}^{(i)}$.
5. Assign importance weight $\hat{w} = f(\hat{x})/f(\bar{\mu})$ to the sampled particle $\hat{x}$.

Algorithm 2: Gibbs sampler for the product of several Gaussian mixtures with an analytic function $f(x)$.

these more sophisticated updates are necessary for graphical models with more expressive priors, such as those used in Section 5.

4. Gaussian Graphical Models

Gaussian graphical models provide one of the few continuous distributions for which the BP algorithm may be implemented exactly [24]. For this reason, Gaussian models may be used to test the accuracy of the nonparametric approximations made by NBP. Note that we cannot hope for NBP to outperform algorithms (like Gaussian BP) designed to take advantage of the linear structure underlying Gaussian problems. Instead, our goal is to verify NBP's performance in a situation where exact comparisons are possible.

We have tested the NBP algorithm on Gaussian models with a range of graphical structures, including chains, trees, and grids. Similar results were observed in all cases, so here we only present data for a single typical 5×5 nearest–neighbor grid (as in Figure 1), with randomly selected inhomogeneous potential functions. To create the test model, we drew independent samples from the single correlated Gaussian defining each of the graph's clique potentials, and then formed a nonparametric density estimate based on these samples. Although the NBP algorithm could have directly used the original correlated potentials, sample–based models are a closer match for the information available in many vision applications (see Section 5).

Given input messages $m_{ut}(x_t) = \{\mu_{ut}^{(i)}, \Lambda_{ut}^{(i)}, w_{ut}^{(i)}\}_{i=1}^M$ for each $u \in \Gamma(t) \setminus s$, construct an output message $m_{ts}(x_s)$ as follows:

1. Determine the marginal influence $\zeta(x_t)$ using equation (8):
   (a) If $\psi_{s,t}(x_s, x_t)$ is a Gaussian mixture, $\zeta(x_t)$ is the marginal over x_t.
   (b) For analytic $\psi_{s,t}(x_s, x_t)$, determine $\zeta(x_t)$ by symbolic or numeric integration.
2. Draw M independent samples $\{\hat{x}_t^{(i)}\}_{i=1}^M$ from the product $\zeta(x_t)\psi_t(x_t, y_t)\prod_u m_{ut}(x_t)$ using the Gibbs sampler of Algorithms 1-2.
3. For each $\{\hat{x}_t^{(i)}\}_{i=1}^M$, sample $\hat{x}_s^{(i)} \sim \psi_{s,t}(x_s, x_t = \hat{x}_t^{(i)})$:
   (a) If $\psi_{s,t}(x_s, x_t)$ is a Gaussian mixture, $\hat{x}_s^{(i)}$ is sampled from the conditional of x_s given $\hat{x}_t^{(i)}$.
   (b) For analytic $\psi_{s,t}(x_s, x_t)$, importance sampling or MCMC methods may be used as appropriate.
4. Construct $m_{ts}(x_s) = \{\mu_{ts}^{(i)}, \Lambda_{ts}^{(i)}, w_{ts}^{(i)}\}_{i=1}^M$:
   (a) Set $\mu_{ts}^{(i)} = \hat{x}_s^{(i)}$, and $w_{ts}^{(i)}$ equal to the importance weights (if any) generated in step 3.
   (b) Choose $\{\Lambda_{ts}^{(i)}\}_{i=1}^M$ using any appropriate kernel size selection method (see [19]).

Algorithm 3: NBP algorithm for updating the nonparametric message $m_{ts}(x_s)$ sent from node t to node s as in equation (2).

For each node $s \in \mathcal{V}$, Gaussian BP converges to a steady–state estimate of the marginal mean μ_s and variance σ_s^2 after about 15 iterations. To evaluate NBP, we performed 15 iterations of the NBP message updates using several different particle set sizes $M \in [10, 400]$. We then found the marginal mean $\hat{\mu}_s$ and variance $\hat{\sigma}_s^2$ estimates implied by the final NBP density estimates. For each tested particle set size, the NBP comparison was repeated 100 times.

Using the data from each NBP trial, we computed the error in the mean and variance estimates, normalized so each node behaved like a unit–variance Gaussian:

$$\tilde{\mu}_s = \frac{\hat{\mu}_s - \mu_s}{\sigma_s} \qquad \tilde{\sigma}_s^2 = \frac{\hat{\sigma}_s^2 - \sigma_s^2}{\sqrt{2}\sigma_s^2} \tag{9}$$

Figure 3 shows the mean and variance of these error statistics, across all nodes and trials, for different particle set

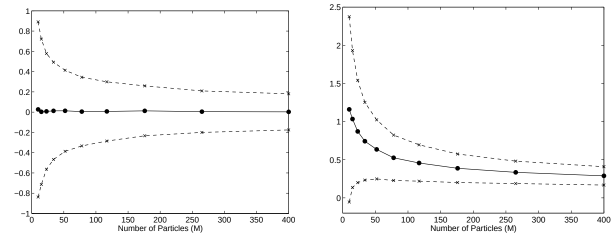

Mean ($\tilde{\mu}_s$) Variance ($\tilde{\sigma}_s^2$)

Figure 3: NBP performance for a 5×5 grid with Gaussian potentials and observations. Plots show the mean (solid line) and standard deviation (dashed line) of the normalized error measures of equation (9), as a function of particle set size M.

sizes M. The NBP algorithm always provides unbiased estimates of the conditional mean, but overly large variance estimates. This bias, which decreases as more particles are used, is due to the smoothing inherent in kernel–based density estimates. As expected for samples drawn from Gaussian distributions, the standard deviation of both error measures falls as $M^{-1/2}$.

5. Component–Based Face Models

Just as particle filters have been applied to a wide range of problems, the NBP algorithm has many potential computer vision applications. Previously, NBP has been used to estimate dense stereo depth maps [20]. However, in this section we instead use NBP to infer relationships between the PCA coefficients in a component–based model of the human face, which combines elements of [14, 23]. Local appearance models of this form share many features with the articulated models commonly used in tracking applications. However, they lack the implementational overhead associated with state–of–the–art person trackers [18], for which we think NBP would also be well suited.

5.1. Model Construction

In order to focus attention on the performance of the NBP algorithm, we make several simplifying assumptions. We assume that the scale and orientation (but not the position) of the desired face are known, and that the face is oriented towards the camera. Note, however, that the graphical model we propose could be easily extended to estimate more sophisticated alignment parameters [5].

To construct a model of facial variations, we used training images from the AR face database [13]. For each of 94 individuals, we chose four standard views containing a range of expressions and lighting conditions (see Figure 4). We then manually selected five feature points (eyes, nose and mouth corners) on each person, and used these points to transform the images to a canonical alignment. These

Figure 4: Two of the 94 training subjects from the AR face database. Each subject was photographed in these four poses.

(a) (b) (c)

Figure 5: PCA–based facial component model. (a) Control points and feature masks for each of the five components. Note that the two mouth masks overlap. (b) Mean features. (c) Graphical prior relating the position and PCA coefficients of each component.

same control points were used to center the feature masks shown in Figure 5(a). In order to model facial variations, we computed a principal component analysis (PCA) of each of the five facial components [14]. The resulting component means are shown in Figure 5(b). For each facial feature, only the 10 most significant principal components were used in the subsequent analysis.

After constructing the PCA bases, we computed the corresponding PCA coefficients for each individual in the training set. Then, for each of the component pairs connected by edges in Figure 5(c), we determined a kernel–based nonparametric density estimate of their joint coefficient probabilities. Figure 6 shows several marginalizations of these 20–dimensional densities, each of which relates a single pair of coefficients (e.g., the first nose and second left eye coefficients). Note that all of these plots involve one of the three most significant PCA bases for each component, so they represent important variations in the data. We can clearly see that simple Gaussian approximations would lose most of this data set's interesting structure.

Using these nonparametric estimates of PCA coefficient relationships and the graph of Figure 5(c), we constructed a joint prior model for the location and appearance of each

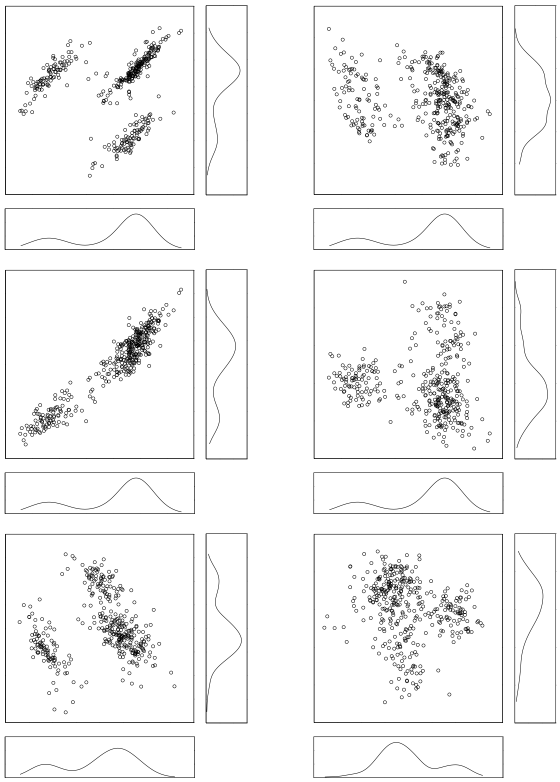

Figure 6: Empirical joint densities of six different pairs of PCA coefficients, selected from the three most significant PCA bases at each node. Each plot shows the corresponding marginal distributions along the bottom and right edges. Note the multimodal, non–Gaussian relationships.

facial component. The hidden variable at each node is 12 dimensional (10 PCA coefficients plus location). We approximate the true clique potentials relating neighboring PCA coefficients by the corresponding joint probability estimates [7]. We also assume that differences between feature positions are Gaussian distributed, with a mean and variance estimated from the training set.

5.2. Estimation of Occluded Features

In this section, we apply the graphical model developed in the previous section to the simultaneous location and reconstruction of partially occluded faces. Given an input image, we first localize the region most likely to contain a face using a standard eigenface detector [14] trained on partial face images. This step helps to prevent spurious detection of background detail by the individual components. We then construct observation potentials by scanning each feature mask across the identified subregion, producing the best 10–component PCA representation $\hat{y}$ of each pixel window y. For each tested position, we create a Gaussian mixture component with mean equal to the matching coefficients, and weight proportional to $\exp\left\{-||y-\hat{y}||^2/2\sigma^2\right\}$. To account for outliers produced by occluded features, we add a single zero mean, high–variance Gaussian to each observation potential, weighted to account for 20% of the total likelihood.

We tested the NBP algorithm on uncalibrated images of individuals not found in the training set. Each message was represented by $M = 100$ particles, and each Gibbs sampling operation used $\kappa = 100$ iterations. Total computation time for each image was a few minutes on a Pentium 4 workstation. Due to the high dimensionality of the variables in this model, and the presence of the occlusion process, discretization is completely intractable. Therefore, we instead compare NBP's estimates to the closed form solution obtained by fitting a single Gaussian to each of the empirically derived mixture densities.

Figure 7 shows inference results for two images of a man concealing his mouth. In one image he is smiling, while in the other he is not. Using the relationships between eye and mouth shape learned from the training set, NBP is able to correctly infer the shape of the concealed mouth. In contrast, the Gaussian approximation loses the structure shown in Figure 6, and produces two mouths which are visually equal to the mean mouth shape. While similar results could be obtained using a variety of ad hoc classification techniques, it is important to note that the NBP algorithm was only provided unlabeled training examples.

Figure 8 shows inference results for two images of a woman concealing one eye. In one image, she is seen under normal illumination, while in the second she is illuminated from the left by a bright light. In both cases, the concealed eye is correctly estimated to be structurally similar to the visible eye. In addition, NBP correctly modifies the illumination of the occluded eye to match the intensity of the corresponding mouth corner. This example shows NBP's ability to seamlessly integrate information from multiple nodes to produce globally consistent estimates.

6. Discussion

We have developed a nonparametric sampling–based variant of the belief propagation algorithm for graphical models with continuous, non–Gaussian random variables. Our parts–based facial modeling results demonstrate NBP's ability to infer sophisticated relationships from training data, and suggest that it may prove useful in more complex visual tracking problems. We hope that NBP will allow the successes of particle filters to be translated to many new computer vision applications.

Acknowledgments

The authors would like to thank Ali Rahimi for his help with the facial appearance modeling application.

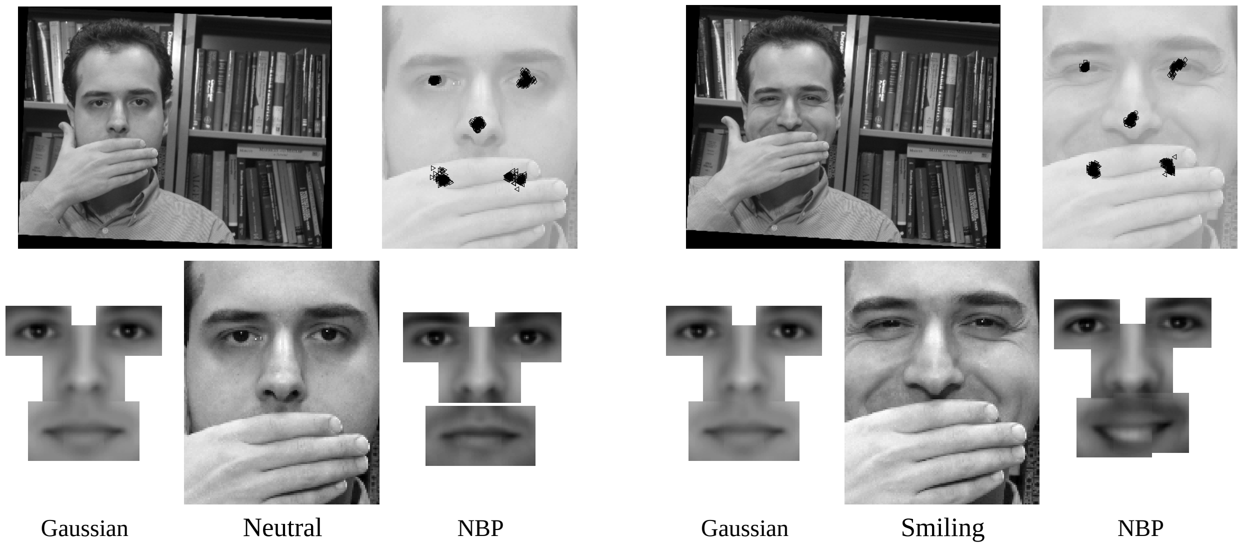

Figure 7: Simultaneous estimation of location (top row) and appearance (bottom row) of an occluded mouth. Results for the Gaussian approximation are on the left of each panel, and for NBP on the right. By observing the squinting eyes of the subject (right), and exploiting the feature interrelationships represented in the trained graphical model, the NBP algorithm correctly infers that the occluded mouth should be smiling. A parametric Gaussian model doesn't capture these relationships, producing estimates indistinguishable from the mean face.

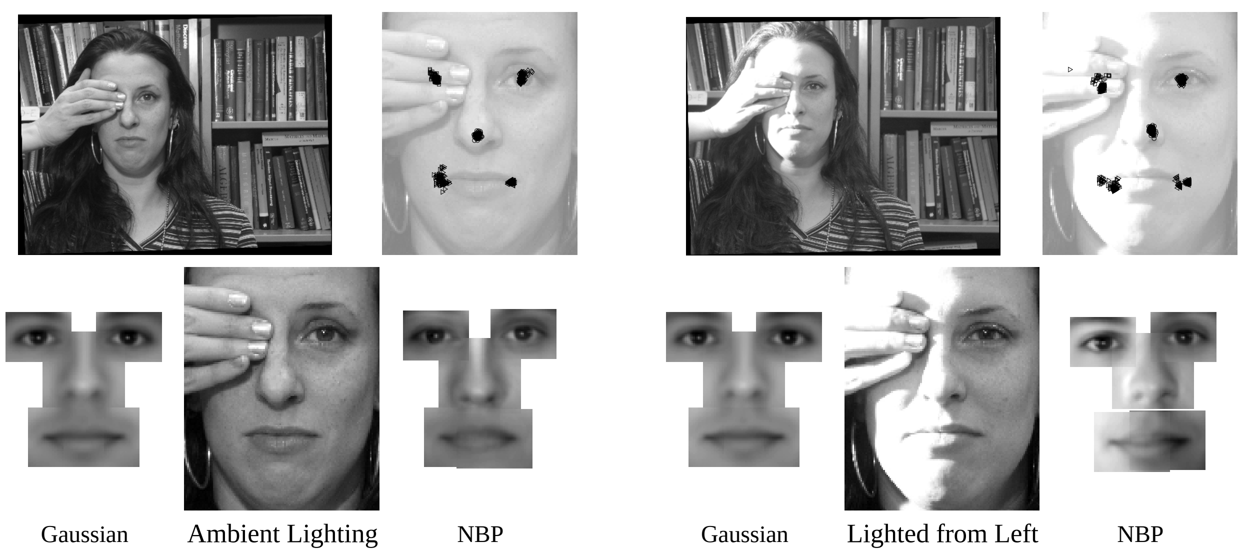

Figure 8: Simultaneous estimation of location (top row) and appearance (bottom row) of an occluded eye. NBP combines information from the visible eye and mouth to determine both shape and illumination of the occluded eye, correctly inferring that the left eye should brighten under the lighting conditions shown at right. The Gaussian approximation fails to capture these detailed relationships.

References

[1] D. L. Alspach and H. W. Sorenson. Nonlinear Bayesian estimation using Gaussian sum approximations. *IEEE Trans. AC*, 17(4):439–448, August 1972.

[2] G. Cooper. The computational complexity of probabilistic inference using Bayesian belief networks. *Artificial Intelligence*, 42:393–405, 1990.

[3] J. M. Coughlan and S. J. Ferreira. Finding deformable shapes using loopy belief propagation. In *ECCV*, pages 453–468, 2002.

[4] A. P. Dawid, U. Kjærulff, and S. L. Lauritzen. Hybrid propagation in junction trees. In *Adv. Intell. Comp.*, pages 87–97, 1995.

[5] F. De la Torre and M. J. Black. Robust parameterized component analysis: Theory and applications to 2D facial modeling. In *ECCV*, pages 653–669, 2002.

[6] A. Doucet, N. de Freitas, and N. Gordon, editors. *Sequential Monte Carlo Methods in Practice*. Springer-Verlag, New York, 2001.

[7] W. T. Freeman, E. C. Pasztor, and O. T. Carmichael. Learning low–level vision. *IJCV*, 40(1):25–47, 2000.

[8] B. J. Frey, R. Koetter, and N. Petrovic. Very loopy belief propagation for unwrapping phase images. In *NIPS 14*. MIT Press, 2002.

[9] S. Geman and D. Geman. Stochastic relaxation, Gibbs distributions, and the Bayesian restoration of images. *IEEE Trans. PAMI*, 6(6):721–741, November 1984.

[10] M. Isard and A. Blake. Contour tracking by stochastic propagation of conditional density. In *ECCV*, pages 343–356, 1996.

[11] D. Koller, U. Lerner, and D. Angelov. A general algorithm for approximate inference and its application to hybrid Bayes nets. In *UAI 15*, pages 324–333, 1999.

[12] S. L. Lauritzen. *Graphical Models*. Oxford University Press, 1996.

[13] A. M. Martínez and R. Benavente. The AR face database. Technical Report 24, CVC, June 1998.

[14] B. Moghaddam and A. Pentland. Probabilistic visual learning for object representation. *IEEE Trans. PAMI*, 19(7):696–710, July 1997.

[15] O. Nestares and D. J. Fleet. Probabilistic tracking of motion boundaries with spatiotemporal predictions. In *CVPR*, pages 358–365, 2001.

[16] E. Parzen. On estimation of a probability density function and mode. *Ann. of Math Stats.*, 33:1065–1076, 1962.

[17] J. Pearl. *Probabilistic Reasoning in Intelligent Systems*. Morgan Kaufman, San Mateo, 1988.

[18] H. Sidenbladh and M. J. Black. Learning the statistics of people in images and video. *IJCV*, 2002. In revision.

[19] B. W. Silverman. *Density Estimation for Statistics and Data Analysis*. Chapman & Hall, London, 1986.

[20] E. B. Sudderth, A. T. Ihler, W. T. Freeman, and A. S. Willsky. Nonparametric belief propagation. Technical Report 2551, MIT Laboratory for Information and Decision Systems, October 2002.

[21] J. Sun, H. Shum, and N. Zheng. Stereo matching using belief propagation. In *ECCV*, pages 510–524, 2002.

[22] M. J. Wainwright, T. Jaakkola, and A. S. Willsky. Tree–based reparameterization for approximate inference on loopy graphs. In *NIPS 14*. MIT Press, 2002.

[23] M. Weber, M. Welling, and P. Perona. Unsupervised learning of models for recognition. In *ECCV*, 2000.

[24] Y. Weiss and W. T. Freeman. Correctness of belief propagation in Gaussian graphical models of arbitrary topology. *Neural Comp.*, 13:2173–2200, 2001.

[25] J. S. Yedidia, W. T. Freeman, and Y. Weiss. Constructing free energy approximations and generalized belief propagation algorithms. Technical Report 2002-35, Mitsubishi Electric Research Laboratories, August 2002.